J Mater Sci (2010) 45:6345–6352
DOI 10.1007/s10853-010-4596-z

IMEC 2009

Study of fracture evolution in copper sheets by in situ tensile test and EBSD analysis

S. Ifergane · Z. Barkay · O. Beeri · N. Eliaz

Received: 12 January 2010 / Accepted: 4 May 2010 / Published online: 18 May 2010

Abstract Microstructural changes during plastic deformation and fracture evolution play an important role in the understanding of fracture mechanisms. However, most publications have focused on the initial stages of deformation where the latter is uniform. The current study was focused on the last stages of fracture, the necking, and crack propagation. Tensile specimens were examined by in situ scanning electron microscope equipped with a tensile module and electron backscatter diffraction. It was demonstrated that the fracture evolution consists of scanty diffuse necking followed by pronounced localized necking, in which the deformation band spread through the width of the specimen in two combined mechanisms—shearing and dimpling. The microstructural changes inside the deformation band adjacent to crack edge were compared to those in the uniform deformation zone. In the deformed areas, the grains became elongated and preferentially orientated in the loading direction. The relative frequency of twin boundaries at 60° was reduced in the deformed areas compared to non-deformed areas, while the misorientations at low angles of 3°–15°, which imply on a dislocation pileups subgrained structure, were increased to greater extent at the crack edge. Inside the deformation band, the amount of deformation was increased compared to the uniformly deformed region with grain fragments as a result of the complexity of stresses, although similar deformation mechanisms were identified.

S. Ifergane · O. Beeri
Nuclear Research Center Negev, P.O. Box 9001, Beer-Sheva 84190, Israel

S. Ifergane · N. Eliaz (✉)
The Materials and Nanotechnologies Program, Tel-Aviv University, Ramat Aviv, Tel-Aviv 69978, Israel
e-mail: neliaz@eng.tau.ac.il

Z. Barkay
The Wolfson Applied Materials Research Centre, Tel-Aviv University, Ramat Aviv, Tel-Aviv 69978, Israel

Introduction

The final stage of fracture is a complicated event associated with a change from uniform deformation to a local instability state. Many models, such as tensile flow instability (necking) and wrinkling, have been suggested to describe the final stages of fracture. One common application of such models is to predict the limits of mechanical forming [1]. In uniaxial tension, the Considère criterion [2] associates the inception of necking with the maximal applied load. Other theories [3] relate the geometry or material defects to initiation of strain localization. For specimens with a rectangular cross-section, there are two types of tensile flow instability [4]. The first type is *diffuse necking*, so called because its extent is much greater than the sheet thickness. Diffuse necking may terminate in fracture, although it is often followed by a second instability process, called *localized necking*, where the neck is a narrow band with a width about equal to the sheet thickness, inclined at an angle to the specimen axis. Localized necking is associated with plane-strain deformation [4]; both the strain and strain rate are increased considerably within the deformation band [5].

In the last decade, great interest has evolved in measuring the mechanical properties and studying the deformation and failure processes in micro- and nano-specimens, for example those made of pure copper [6–14]. Unfortunately, the study of the mechanical behavior of thicker specimens, including sheets (thickness between

0.15 and 6.33 mm), by advanced characterization techniques has often been overlooked. For example, the use of a tensile stage in a scanning electron microscope (SEM) enables to observe surface deformation at high magnifications and correlate it with the force–displacement curve (or stress–strain curve, if the specimen dimensions are known precisely and a technique such as digital image correlation is used to determine the local strain field), which is acquired simultaneously. This combination is powerful for observing slip bands and necking as well as identifying the crack origin in real-time and video recording the crack propagation. The use of an environmental scanning electron microscope (ESEM) may be useful in studying non-conducting or wet materials. Complimentary electron backscatter diffraction (EBSD) analysis allows determining microstructural features such as grain size distribution, phase maps, orientation maps, deformation maps, and boundary misorientation distribution, thus revealing the processes responsible for deformation and fracture evolution.

The plastic deformation and fracture evolution in pure copper sheets have been studied only to limited extent by in situ tensile test combined with EBSD. In most of those cases, the focus was on the *initial* stages of deformation [15, 16], with no reference to diffuse necking and localized necking. Scheriau and Pippan [17] used SEM–EBSD to study sheets of copper, nickel, and iron with grain sizes varying between 100 nm and 100 μm and found that orientation changes in grains larger than 1 μm during uniaxial tensile deformation differed significantly from the behavior in materials with finer grains. The mechanical properties (i.e., the force–displacement curves), however, were not reported. Simons et al. [18] tensile tested both cold-rolled and annealed copper foils and sheets. The samples failed by forming a neck in the thickness direction. Neither the EBSD characterization nor the SEM imaging in that work was done simultaneously with the mechanical testing. Kamaya et al. [19] deformed by tensile test sheets of pure copper and monitored the evolution of surface strain by means of a CCD camera and digital image correlation. SEM–EBSD was subsequently used to map the strains. The distribution of the misorientation within grains tended to be highest near the grain boundaries. Hong et al. [20] subjected cylindrical samples made of fully recrystallized pure copper to dynamic plastic deformation and subsequently used SEM–EBSD to study the grain orientation dependence of deformation twinning. The occurrence of deformation twins in grains with a specific orientation was explained in terms of a Schmid factor analysis. Borbély et al. [21] measured the stress–strain curve for copper single crystals and subsequently used ESEM–EBSD to investigate the local crystallographic orientation.

The objective of this work was to study the microstructural changes, which occur in different regions of specimens made of pure copper sheets loaded until fracture, by means of in situ tensile testing in an ESEM and complementary EBSD analysis. The emphasis was on the *final* stages of deformation, namely localized necking and crack propagation.

Experimental procedure

Flat uniaxial tensile specimens were formed by punch from a sheet made of pure copper (99.99%). The gauge section of the specimen was 15-mm long, 4-mm wide, and 0.2-mm thick. The specimens were annealed in argon at 600 °C for 30 min. The tensile specimens were mechanically polished down to 1 μm diamond paste before testing. Metallurgical cross-sections were observed under a light microscope after chemical etching in a solution composed of 100 mL ethanol, 2 mL HCl, and 5 g $FeCl_3$.

The tensile tests were conducted in a Quanta 200 FEG ESEM from FEI while recording the surface (top view) deformation and crack propagation, both as a movie and as a series of digital still images. A Kammrath & Weiss tensile/compression module was used. This rigid module was designed to work with up to ±5,000 N. The screw tensile tester is driven by a tacho motor and controlled directly from a microprocessor controller or a PC with DDS32 software package. The specimens were gripped with "lath-like" clamps. As both grippers move at the same speed, somewhere in the middle of the specimen the surface stands almost perfectly still, thus enabling high-quality video recording. The load was measured by a 200 N calibrated load cell. The displacement (elongation) measurements were recorded by an LVDT. The displacement speed was 10 μm/min.

Fractography was done following the end of the tensile test. In addition, the fractured specimens were prepared for EBSD analysis by mechanical polishing followed by electropolishing in a solution composed of 2:3 H_2O:H_2PO_4 (85 vol.%) at 2 V for 1 min, using a stainless steel cathode. For EBSD analyses, a HKL-Oxford Channel 5 system with Nordlys II detector was used. The following operation conditions were maintained: scan area 54 × 40 μm, spatial resolution 0.5 μm, working distance 15 mm, inclination relative to the main beam 70°.

Results

A typical engineering stress-strain curve is shown in Fig. 1a. It should be noted that strain values were calculated based on the displacement of the clamps. Mean and

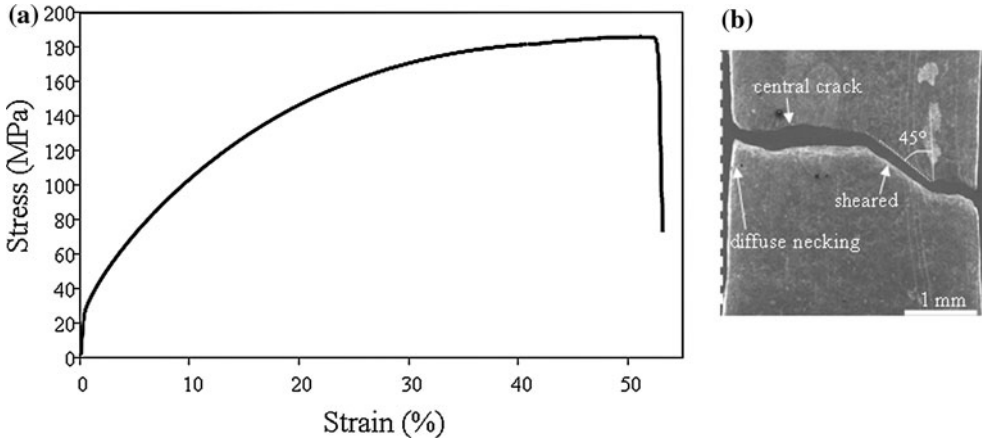

Fig. 1 Stress versus strain curve obtained in a uniaxial tensile test of copper sheet (**a**) and top-view SEM image of the fractured specimen (**b**)

Table 1 Yield stress, ultimate tensile stress, and fracture strain values (mean ± standard deviation) obtained in five in situ tensile tests and compared to typical values reported in [20]

	σ_{yp} (MPa)	σ_{uts} (MPa)	ε_f (%)
Measured in this work	34 ± 4	191 ± 5	49 ± 0.4
Reported in [20]	34	209	60

standard deviation values of the yield stress, ultimate tensile stress, and fracture strain are summarized in Table 1. These values are the product of five tests and reflect good repeatability. The curve in Fig. 1a is characterized by a yield stress, which is significantly lower than the ultimate tensile stress. The ductile behavior is typical of copper, with significant uniform strain before the ultimate tensile stress is reached, followed by a drastic load drop due to instability necking and final rupture. The steep slope within the uniform strain region indicates a relatively high strain-hardening coefficient, while the low-yield stress value indicates that the specimen is fully annealed. SEM image of the fractured specimen right after failure (Fig. 1b) shows some diffuse necking as well as a crack propagation path consisted of both perpendicular and inclined regions with respect to the loading direction.

Figure 2 reveals the microscopic features of fracture evolution under various loads. The images in this figure were selected from a large series of consecutive images acquired at small time intervals. The plastic deformation band (Fig. 2a, b) was originated at the side wall of the specimen and spread along its width. The band height was approximately 0.2 mm (see Fig. 2b), equal to the sheet thickness, as reported in [4] for localized necking. Closer examination reveals that the grains are elongated within the plastic deformation band in the loading direction and that slip lines are present as a result of dislocation motion inside the grains. The deformation band expanded to about 0.5 mm along the specimen's width (Fig. 2f) before shear lips were observed in the front of the spreading band (Fig. 2c). At the second stage of fracture evolution, a crack was initiated approximately at the half height of the deformation band and grew along it (Fig. 2d, e); shear lips appeared at its edge (Fig. 2e). The third stage of fracture evolution started with fast crack propagation along the shear lips (Fig. 2g, h). The shear crack propagation at an inclination angle of 45° was accompanied by the development of shearing dimples (Fig. 2i). After the shear crack arrested, additional deformation was developed in front of the crack to allow perpendicular dimple crack propagation (marked by arrow in Fig. 2g). Thus, crack propagation was assembled from the two competitive crack propagation mechanisms—shearing and dimpling.

Fractography revealed that the perpendicularly oriented crack surface contained ductile dimples in the middle zone of the sheet thickness (Fig. 3a) and an inclined sheared zone close to the exterior. The ductile dimples are characteristic of a plane-strain fracture mode. In contrast, the shear cracks are related to a plane-stress fracture mode and showed no ductile dimples (Fig. 3b).

Electron backscatter diffraction analysis was carried out at the top surface of the fractured specimen after mechanical and electrochemical polishing. The three zones that were characterized are marked in Fig. 4a. The first zone, at the edge of the grip section, was not deformed during the tensile test and can therefore be regarded as "annealed." The second zone, approximately 2 mm far from fracture, experienced uniform deformation during the tensile test. The third zone was at the edge of the crack, where ductile dimples were observed, in the localized deformation band. The microstructure of the annealed copper consisted of a face centered cubic (FCC) matrix, with grain size of about 150 μm and high frequency of annealing twins (Fig. 4b).

The EBSD results are presented in Fig. 5a–c in terms of the Euler angle maps. The microstructure of the annealed zone in Fig. 5a is similar to that shown in Fig. 4b. Within

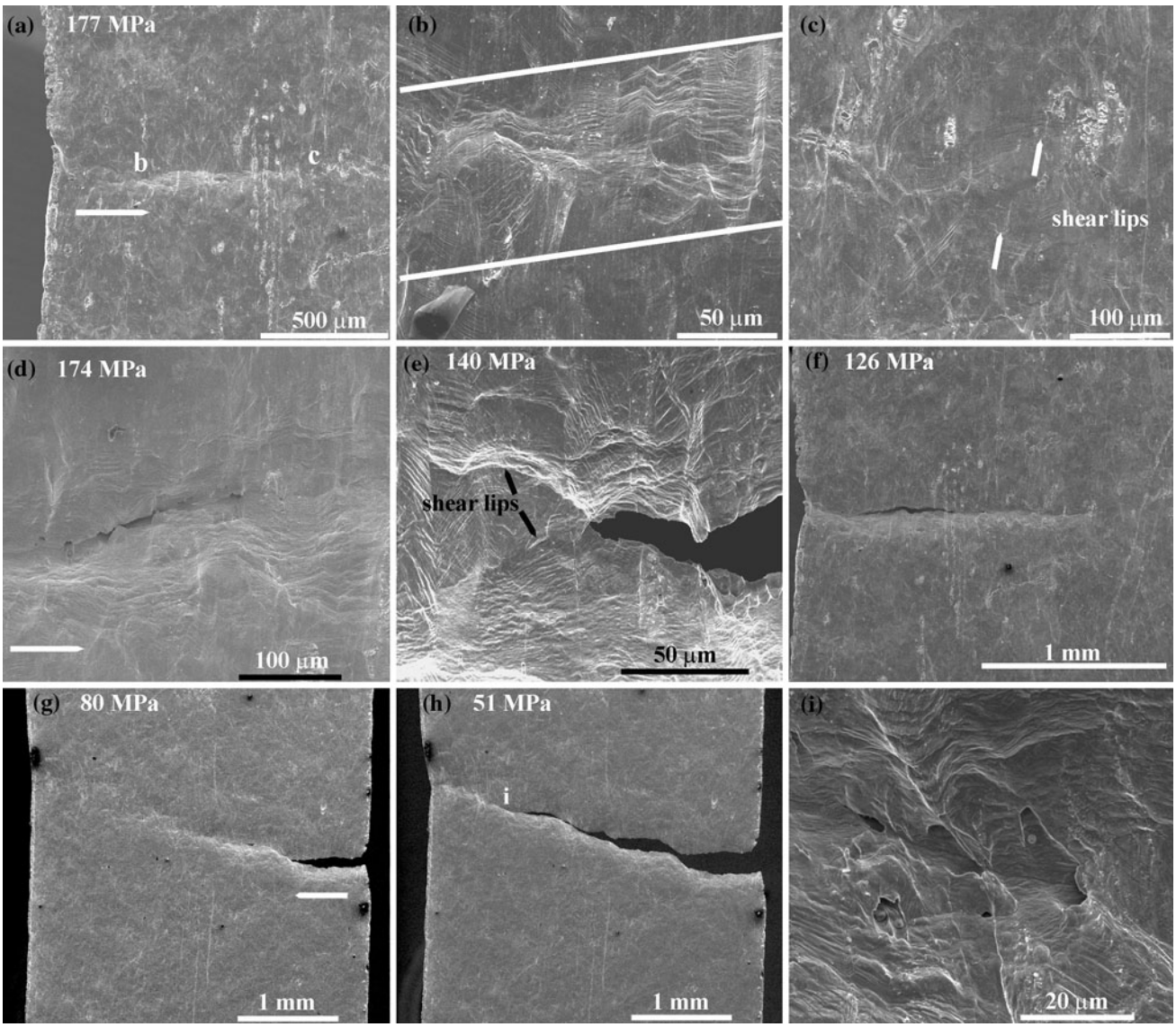

Fig. 2 In situ SEM imaging while tensile testing. The stress corresponding to each image is noted. **a**–**c** Initiation of localized necking and slip lines, with zoom-in on the deformation band (**b**) and shear lips at the crack edge (**c**), **d** evolution of the central crack, **e** shear lips at the edge of the central crack, **f** the central crack, **g**, **h** final fracture in another specimen, **i** shearing and formation of shear dimples around a central crack

the deformed zone, grains elongated along the *Y*-direction were noticed in the Euler map (see Fig. 5b). The Σ3 coincident site lattice (CSL) twin boundaries are marked in yellow. They are known as "annealing twins" and are formed by 60° rotation about <111> [15]. The misorientation angle distributions along selected lines in Fig. 5a–c are shown in Fig. 5d–f, respectively. Boundaries at a misorientation angle of 60° are characteristic of twinning on the {111} planes. The relative frequency of different misorientation angles is presented in Fig. 5g. The 60° twin boundary was most frequent in the annealed zone. Within the deformed zones, the twinning frequency was significantly reduced, whereas the relative frequency of the 3°–15° low-angle interfaces was increased with deformation level. The annealed zone contained also high frequency of 1°–2° misorientation, which indicates a highly ordered material. The 1°–2° misorientation frequency decreased as the deformation level was increased.

Figure 6 further emphasizes the crystallographic texture in terms of the pole figures. The projections are contoured at multiples of uniform distribution (MUD). The preferred orientation in the deformed regions is thus emphasized along the *Y*-axis, which was parallel to the loading direction. Three different crystallographic planes were analyzed, and they all became oriented along the *Y*-axis in a similar way. This behavior is characteristic of the isotropy of the

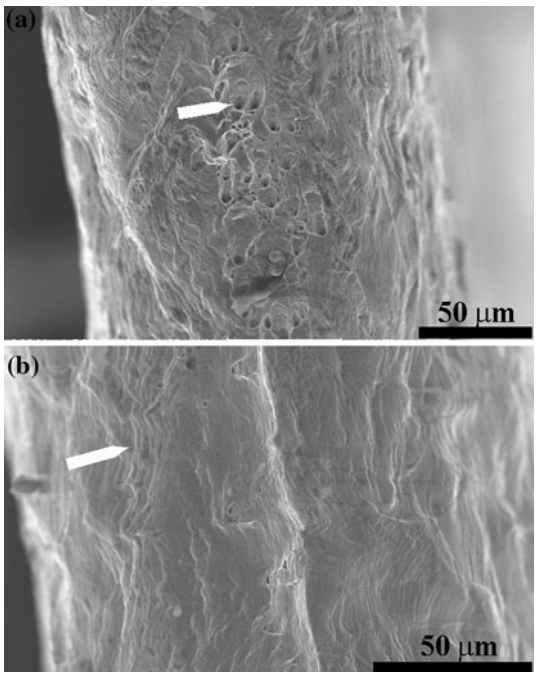

Fig. 3 Fractography (SEM) revealing dimpling in the middle zone of the sheet thickness within the central crack zone (**a**) and an inclined sheared zone with slip lines but no ductile dimples (**b**)

cubic crystal. The preferred orientation was most distinct near the crack edge, whereas a more random orientation was evident in the annealed zone.

Discussion

In this work, in situ tensile testing in the SEM and complementary EBSD analysis enabled determination of the mechanical properties of pure copper sheets, monitoring of the fracture evolution process, and comparison of the microstructural changes inside the deformation band at the crack edge to those in the uniform deformation zone and in the annealed zone. Two major factors significantly affect the fracture event—the high ductility of pure copper (see Table 1) and the geometry of the specimen (1:20 thickness-to-width ratio). These two factors play an important role in the competition between diffuse and localized necking. In situ SEM imaging revealed a scanty diffuse necking followed by a pronounced localized necking. Examination of the localized necking evolution revealed spreading of the deformation band through the width of the specimen (Fig. 2). The crack propagation was found to consist of two mechanisms—shearing and dimpling (Figs. 2 and 3). The dimpled fracture expanded under a high component of plane-strain, perpendicularly to the loading direction, and exhibited ductile dimples at the center of the specimen thickness. While the deformation band formed, ductile dimples formed within the specimen thickness and coalesced to form the crack. In contrast, the shearing plane-stress cracking mode was responsible for crack inclination at 45° relative to the loading axis.

Electron backscatter diffraction analyses illustrated the microstructural changes during plastic deformation. In the annealed zone, a relatively high fraction of 60° interfaces were noticed, characteristic of annealing twins in FCC metals and alloys [22]. The annealed zone contained high frequency of 1°–2° misorientation angles. It has been reported [23] that high fraction of 60° misorientation angle and low fraction of 3°–15° misorientation angles exist in AISI 304 stainless steel that is not fully annealed. In this work, however, it seems that the copper specimens were fully annealed, as there was negligible fraction of low-angle misorientation, the yield stress was fairly low (Table 1) and the pole figure exhibited random orientation (Fig. 6a). EBSD analysis also reflected the different levels of deformation, at or away from the crack edge.

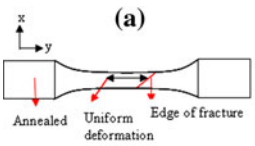

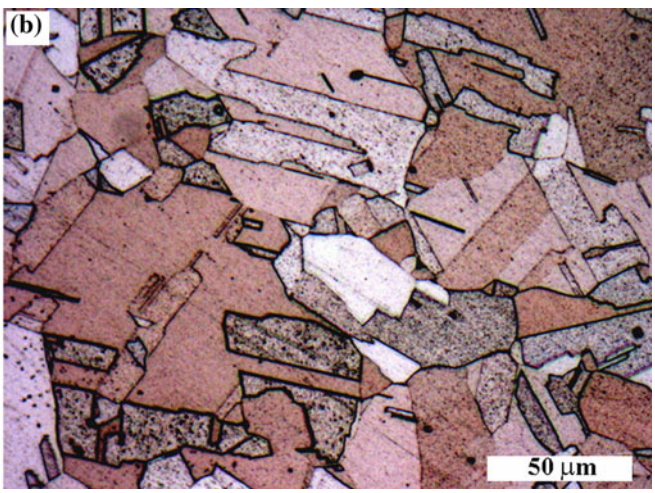

Fig. 4 Schematic illustration of the three zones characterized by EBSD (**a**) and the microstructure of annealed copper as revealed in a chemically etched metallographic cross-section (**b**)

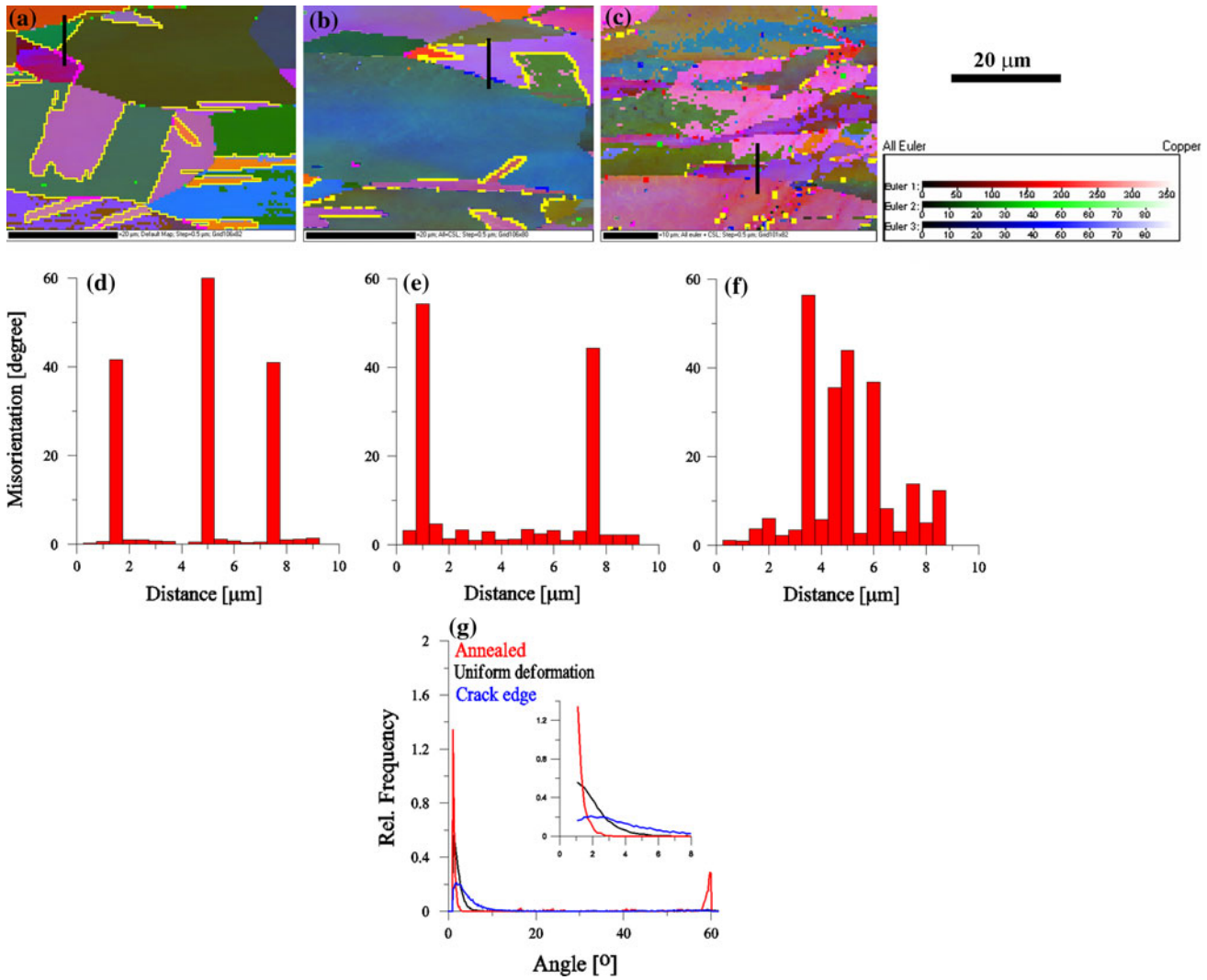

Fig. 5 Euler angle maps acquired within the annealed zone (**a**), uniform deformation zone (**b**), and crack edge zone (**c**). The maps are colored as a mixture of the three Euler angles according to the accompanying key. The *scale bar* for these three maps is provided above the color key. The Σ3 boundaries are marked in *yellow* (*bright*). The misorientation distributions along the *black* (*dark*) *lines* in **a**–**c** are drawn in **d**–**f**, respectively. The relative frequency of misorientations is also compared with respect to the three analyzed zones (**g**)

At the crack edge, the grains were more deformed and directed along the loading direction than within the uniform deformation zone. A similar trend in preferred orientation has been observed in the pole figure of 60% reduction cold-rolled copper specimens compared to randomly oriented annealed copper [24], although rolling is associated with a different deformation mechanism than in mode-I tensile testing.

The relative frequency of low-angle boundaries was higher at the crack edge than within the uniform deformation zone. It is thus assumed that the stress state at the crack edge was more complex than pure uniaxial stresses. Hence, the grains rotated under the complex loading and became elongated with more grain fragments. Within the deformed regions, the frequency of very low-angle (1°–2°) misorientation dramatically decreased as the deformation was increased, indicating on a sub-grained structure and dislocation activity.

The microstructural changes were not homogeneous in all grains; some grains were dramatically changed while others seemed almost unchanged. In each grain, slip will begin when the shear stress on the shearing direction reaches a critical value, namely the critical resolved shear stress (CRSS), as demonstrated for irradiated AISI 316L at various temperatures [25]. Therefore, in each grain the mechanism of failure is different according to the orientation with respect to loading direction, according to Schmid [26].

Misorientation analyses revealed that in the deformed regions (Fig. 5g), the relative frequency of the 60° twins

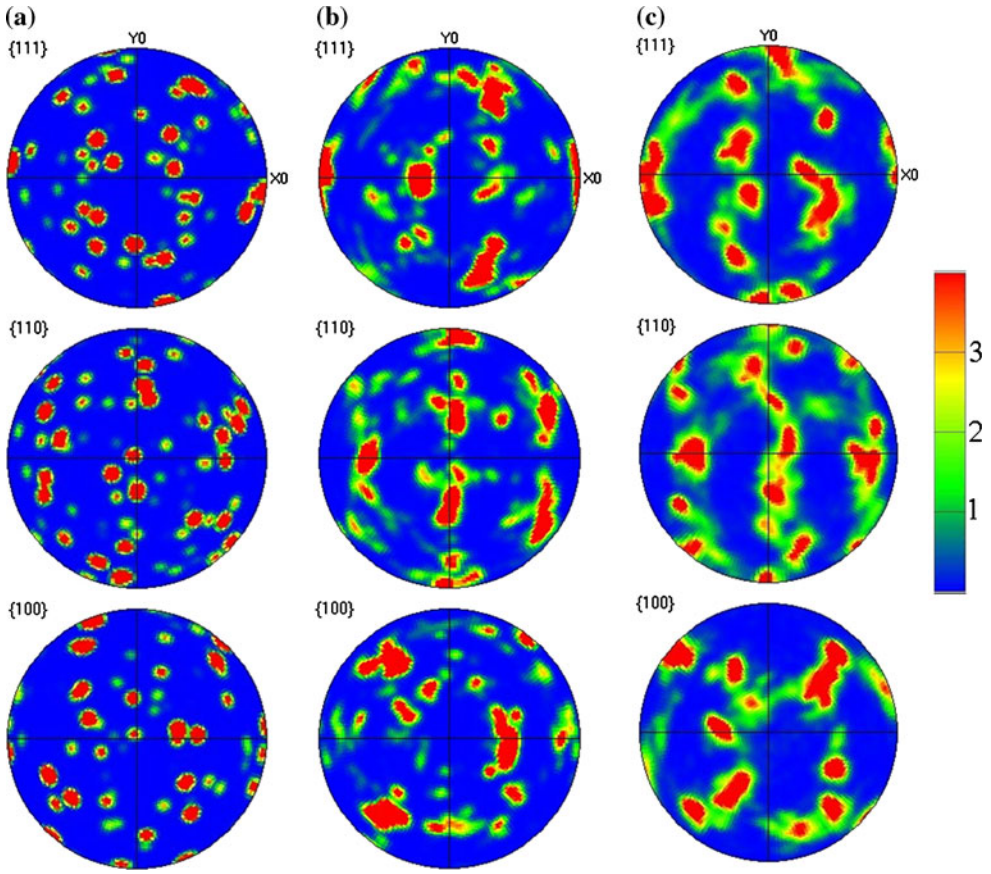

Fig. 6 Pole figures acquired within the annealed (**a**), uniformly deformed (**b**), and crack edge (**c**) zones

was reduced while the relative frequency of the low-angle boundaries (3°–15°) was gradually increased. It may thus be questioned why less twin boundaries are evident in the deformed areas: do the twins "dissolve" during deformation by acting as dislocation sources, does failure occur along twin-free regions which are softer, or is it another mechanism responsible for this phenomenon? For a fully annealed copper, it has been reported [16, 27] that during the *early stages* of deformation, annealing twin boundaries serve as major sources for dislocations in a non-regenerative manner, namely they disappear while producing Shockley partial dislocations. This phenomenon was reflected by a reduction in the overall fraction of the Σ3 boundaries in the EBSD images during deformation. If so, the stress state with respect to the twin orientation and the character of the twin boundary itself will determine whether this boundary will serve as a dislocations source. Other scenarios are that the deformation in the grain occurs by dislocation slip systems remote from twins, or migration of the twin as a result of dislocation pileups [15]. In contrast, for *larger strains*, it has been proposed that twin boundaries may be effective barriers to dislocation motion, establishing dislocation pileups and crack nucleation sites [27, 28]. It is our belief that the results of the present study support the twin dissolution mechanism also during the *final stages* of deformation. This could be related either to dissociation into partial dislocations, as suggested before for the *initial stages* of deformation, or to destabilization of the twin boundary by dislocations that move under the applied force and approach it. However, further experimental and modeling work is required before a definite mechanism can be suggested.

Conclusions

The annealed copper flat specimen exhibited typical ductile behavior during uniaxial tensile test, with low yield stress, significant strain-hardening during uniform strain before ultimate tensile stress, followed by a drastic load drop due to instability necking and final rupture.

Fracture evolution consisted of limited diffuse necking followed by pronounced localized necking, in which deformation band spread through the width of the specimen. Dimpled crack in perpendicular to loading direction initiated in the middle of the deformation band and spread

along it, combined with sheared cracking inclined at 45° to the loading direction.

The microstructural changes inside the deformation band at the crack edge were characterized in comparison to those in the uniform deformation zone and in the annealed zone. Inside the deformation band, the grains became more elongated and preferentially orientated in the loading direction, with grain fragments resulting from the complexity of stresses. The amount of deformation in the deformation band adjacent to fracture increased relative to the uniform deformation zone, although similar deformation mechanisms were identified.

A misorientation of 60°, which was highly frequent in the annealed condition, was infrequent in the deformed state, indicating that the twins were "dissolved." The frequency of the misorientations of 3°–15°, which are characteristic of a dislocation pileups subgrained structure, increased with deformation level.

Acknowledgements The authors thank O. Sabag, S. Levi, G. Agronov, M. Shohat, I. Maidani, M. Chunnin, and I. Benishti for their technical assistance.

References

1. Korhonen AS, Manninen T (2008) Mater Sci Eng A 488:157
2. Considère A (1885) Ann Ponts Chaussées 9:574
3. Marciniak Z, Kuczynski K (1967) Int J Mech Sci 9:609
4. Dieter GE (1988) Mechanical metallurgy. McGraw-Hill Book Co, London
5. Hill R (1952) J Mech Phys Solids 1:19
6. Wang YM, Wang K, Pan D, Lu K, Hemker KJ, Ma E (2003) Scr Mater 48:1581
7. Huang H, Yu DW, Verdier M, Spaepen F (2003) Int J Fract 119/120:359
8. Kumar KS, Van Swygenhoven H, Suresh S (2003) Acta Mater 51:5743
9. Volinsky AA, Gerberich WW (2003) Microelectron Eng 69:519
10. Hansen N (2004) Scr Mater 51:801
11. Connolley T, Mchugh PE, Bruzzi M (2005) Fatigue Fract Eng Mater Struct 28:1119
12. Zhou ZM, Zhou Y, Yang CS, Chen JA, Ding W, Ding GF (2006) Sens Actuator A 127:392
13. Kiener D, Grosinger W, Dehm G, Pippan R (2008) Acta Mater 56:580
14. Dehm G (2009) Prog Mater Sci 54:664
15. Brown JA, Ghoniem NM (2009) Acta Mater 57:4454
16. Flinn JE, Field DP, Korth GE, Lillo TM, Macheret J (2001) Acta Mater 49:2065
17. Scheriau S, Pippan R (2008) Mater Sci Eng A 493:48
18. Simons G, Weippert Ch, Dual J, Villain J (2006) Mater Sci Eng A 416:290
19. Kamaya M, Quinta Da Fonseca J, Li LM, Preuss M (2007) Appl Mech Mater 7–8:173
20. Hong CS, Tao NR, Lu K, Huang X (2009) Scr Mater 61:289
21. Borbély A, Szabó PJ, Groma I (2005) Mater Sci Eng A 400–401:132
22. Askeland DR (1994) The science and engineering of materials, 3rd edn. PWS Publishing Company, Boston
23. El Wahabi M, Gavard L, Cabrera JM, Prado JM, Montheillet F (2005) Mater Sci Eng A 393:83
24. Lefevre-Schlick F, Brechet Y, Zurob HS, Purdy G, Embury D (2009) Mater Sci Eng A 502:70
25. Wu X, Pan X, Mabon JC, Li M, Stubbins JF (2007) J Nucl Mater 371:90
26. Schmid E (1931) Z Electrochem 37:447
27. Field DP, True BW, Lillo TM, Flinn JE (2004) Mater Sci Eng A372:173
28. Armstrong RW, Codd I, Douthwaite RM, Petch NJ (1962) Philos Mag 7:45